Dynamical investigation of a linear motor to be used in cellular phones

Attila Lukács / *Zsolt* Szabó

Abstract

Nowadays vibrating alert is a common feature of cellular phones. For this purpose a radial flux linear-motor with air-gap solenoid was developed, which operates in the vicinity of its natural frequency. This paper presents the amplification diagram of the mechanical model of this new construction obtained both numerically and analytically. Furthermore, the results are compared to measurement data which are showing nonlinear dynamical behaviour.

Keywords

electromagnetic actuator · vibrating alert · forced Duffing equation

Attila Lukács

Department of Mechatronics, Optics and Instrumentation Technology, BME, H-1111 Budapest, Műegyetem rkp. 5., Hungary
e-mail: lukacs@mogi.bme.hu,

Zsolt Szabó

Department of Applied Mechanics, BME, H-1111 Budapest, Műegyetem rkp. 5., Hungary
e-mail: szazs@mm.bme.hu

1 Introduction

Electromagnetic actuators rotate shafts, force masses for periodic translational motion. They can be used for both interrupted and stationary working. The actuator itself is an electro-mechanical (or mechatronical) system in which the moving mechanical part has a feed-back on the operating electronic circuit [4, 6]. In the simplest case, such an actuator has one mechanical and one electrical degree of freedom [1]: the position of the moving mass and the electric current in the circuit. However, the equation of motion of the mass is a second order differential equation due to *Newton's Second Law* while *Kirchhoff's Voltage Law* yields a first order differential equation at the most.

Fig. 1. Photo of the investigated electro-magnetic actuator

Fig. 1 shows the mechatronical construction in question. Its size is in the mm-range. The main application field is to create mechanical excitation in cellular phones [2, 5, 7]. The actuator in the picture was made by the authors as the prototype of a radial flux linear motor with air-gap solenoid.

2 System model of the electro-magnetic actuator

In Fig. 2 an exploded sketch of the actuator can be seen. The permanent magnet (NdFeB), the bell-shaped flux-closing part and the ring-shaped air-gap build the magnetic circuit which is, at the same time, the moving part of the actuator. Fixing it on a flexible suspension yields a one-degree-of-freedom oscillator

of which mass m is only 1 gramm. The electric circuit contains the solenoid coil and the excitation voltage source $U(t)$. The coil has n turns of length l. The electro-mechanical model is shown in Fig. 3. The resistor R and the inductor L take into consideration the resistance and the self-inductance of the coil.
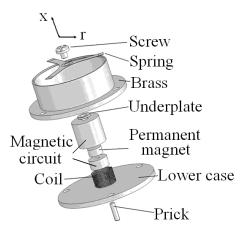

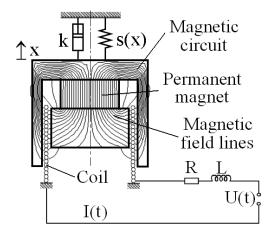
Fig. 2. Exploded sketch of the actuator

Fig. 3. Mechatronical system model

This system has three state variables: position $x(t)$ and velocity $\dot{x}(t)$ of the mass m, and current $I(t)$ of the electric circuit. The governing equations according to *Newton's Second Law* and *Kirchhoff's Voltage Law* are as follows:

$$m\ddot{x} = -F_s(x) - k\dot{x} + F_B(I), \quad (1)$$
$$L\dot{I} + U_B(\dot{x}) + RI = U(t), \quad (2)$$

where $F_s(x)$ is the nonlinear spring force, k is the damping coefficient of the mechanical part, and $F_B(I)$ is the *Lorentz force* reacting on the magnet from the coil containing current I in a magnetic field of induction B:

$$F_B(I) = -I(nl\mathbf{e}_t) \times (B\mathbf{e}_r) \cdot \mathbf{e}_x \equiv InlB, \quad (\mathbf{e}_r\mathbf{e}_t\mathbf{e}_x = 1) \quad (3)$$

because the current in the turns of the coil is perpendicular to the radial magnetic field in the air-gap ($\mathbf{e}_r$, $\mathbf{e}_t$ and $\mathbf{e}_x$ denote the radial, tangential and axial unit vectors, respectively). The formula $U_B(\dot{x})$ represents the counter electromotive force which is induced by the moving permanent magnet:

$$U_B(\dot{x}) = \dot{x}nlB. \quad (4)$$

The spring force was assumed to have cubic nonlinearity: $F_s(x) = s(x + \mu x^3)$, because of the small dimensions of the suspension spring (its thickness is only 50 μm) and its relatively "large" deformation (it can be even 0.25 mm). The linear spring stiffness s and the coefficient μ of the nonlinear term was determined both by finite element analysis using ANSYS and experimentally. The results are in good agreement, as it is shown in Fig. 4. The function fitted on the experimental data is as follows:

$$F_s(x) = 0.51 \left[\frac{N}{mm}\right] (x + 26 \left[mm^{-2}\right] x^3). \quad (5)$$
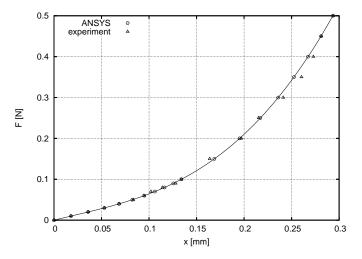

Fig. 4. Nonlinear characteristic of the spring force

Substituting formulas (3), (5) and (4) into Eq. (1) and Eq. (2) respectively, we obtain the following differential equations:

$$\ddot{x} + 2D\alpha\dot{x} + \alpha^2(x + \mu x^3) = \frac{1}{m}BlnI, \quad (6)$$
$$L\dot{I} + Bln\dot{x} + RI = U_0 \cos\omega t, \quad (7)$$

where $\alpha^2 = s/m$, $2D\alpha = k/m$ and $U_0 \cos\omega t$ is the sinusoidal excitation voltage of a low-frequency generator. The experimentally determined values of system parameters are summarized in Table 1.

Because of its small value, the inductance can be neglected. This assumption was confirmed by numerical simulations, *i.e.* it is satisfactory considering only the following second order differential equation:

$$\ddot{x} + \left(2D\alpha + \frac{(Bln)^2}{mR}\right)\dot{x} + \alpha^2(x + \mu x^3) = \frac{Bln}{mR}U_0 \cos\omega t. \quad (8)$$

Fig. 5 shows the obtained amplification diagram $A(\omega)$ of system (8) and the relative error comparing to the simulation results $A_L(\omega)$ where the inductance L was taken into account:
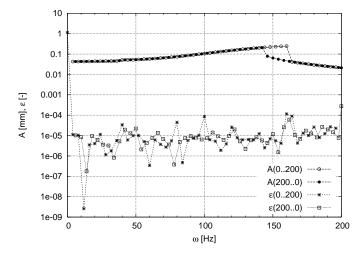
$$\varepsilon(\omega) = \frac{|A(\omega) - A_L(\omega)|}{A_L(\omega)}.$$

System parameter	Value
mass:	$m = 0.001$ kg
relative damping:	$D = 0.065$
angular eigenfrequency:	$\alpha = 714$ rad/s = 114 Hz
nonlinear spring coefficient:	$\mu = 26 \times 10^6$ 1/m^2
number of turns:	$n = 30$
length of a turn:	$l = 0.014$ m
magnetic induction*:	$B = 0.22$ T
resistance:	$R = 10\ \Omega$
inductance:	$L = 0.053$ mH
amplitude of the excitation voltage:	$U_0 = 2.46$ V

(*: obtained numerically using ANSYS)

It can be seen that the error is small relative to the vibration amplitude, thus it can be neglected, indeed.

Fig. 5. Simulated amplification diagram (A [mm]) and its relative error (ε) w.r.t. the original system ($0 \to 200$: for increasing frequencies, $200 \to 0$: for decreasing frequencies)

3 Analytical investigations

Eq. (8) is a forced damped Duffing equation with cubic non-linearity. For the sake of simplicity, we neglect the effect of damping:

$$\ddot{x} + \alpha^2 x(1 + \mu x^2) = \alpha^2 f_0 \cos \omega t, \qquad (9)$$

where

$$f_0 = \frac{Bln}{\alpha^2 mR} U_0 \approx 0.045 \text{ [mm]}.$$

3.1 Autonomous case

If there is no excitation ($f_0 = 0$), according to Poincaré's method of small parameters [3] the solution can be assumed as

$$x(t) = x_0 \cos(\gamma t + \delta) + \mu x_1(t) + O(\mu^2), \qquad (10)$$

where

$$\gamma = \alpha + \mu h_1 + O(\mu^2) \qquad (11)$$

is the modified angular eigenfrequency and h_1 is an unknown parameter, which can be determined as follows.

Let us consider only the solution belonging to the following initial conditions:

$$x(0) = x_0, \quad \dot{x}(0) = 0, \quad (x_1(0) = 0, \ \dot{x}_1(0) = 0, \ \cdots) \quad (12)$$

which implies $\delta = 0$.

Now, Eq. (9) can be rewritten as

$$\ddot{x} + (\gamma - \mu h_1)^2 x(1 + \mu x^2) \approx 0, \qquad (13)$$

and if we put (10) into (13) and separate the coefficients of μ it yields:

$$\mu^0: \quad (-\gamma^2 + \gamma^2)x_0 \cos \gamma t = 0,$$
$$\mu^1: \quad \ddot{x}_1(t) + \gamma^2 x_1(t) = 2h_1 \gamma x_0 \cos \gamma t - \gamma^2 x_0^3 \cos^3 \gamma t,$$
$$\mu^2: \quad \cdots$$

Since

$$\cos^3 \gamma t = \frac{1}{4} \cos 3\gamma t + \frac{3}{4} \cos \gamma t,$$

and the resonant solution should be avoided, the coefficient of $\cos \gamma t$ has to be zero in the equation belonging to μ^1, *i.e.*

$$2h_1 \gamma x_0 - \frac{3}{4} \gamma^2 x_0^3 = 0 \quad \Rightarrow \quad h_1 = \frac{3}{8} \gamma x_0^2. \qquad (14)$$

Thus, the base frequency can be obtained from formulas (11) and (14):

$$\gamma \approx \frac{\alpha}{1 - \frac{3}{8}\mu x_0^2} = \frac{114}{1 - \frac{3}{8}26 \cdot 0.1^2} \equiv 126 \text{ [Hz]}. \qquad (15)$$

The solution that satisfies the initial conditions (12) for $x_1(t)$ is

$$x_1(t) = \frac{x_0^3}{32}(\cos 3\gamma t - \cos \gamma t),$$

hence,

$$x(t) = (x_0 - \mu \frac{x_0^3}{32}) \cos \gamma t + \mu \frac{x_0^3}{32} \cos 3\gamma t + O(\mu^2).$$

3.2 Nonautonomous case

Let us rewrite Eq. (9) into dimensionless form:

$$x'' + x(1 + \mu x^2) = f_0 \cos \lambda \tau, \qquad (16)$$

where $\tau = \alpha t$ is the dimensionless time, $'$ denotes $d/d\tau$ and $\lambda = \omega/\alpha$ is the frequency ratio.

The particular solution of the linearized system ($\mu = 0$):

$$x(\tau) = \frac{f_0}{1 - \lambda^2} \cos \lambda \tau. \qquad (17)$$

After some trigonometric considerations (*e.g.* $\cos^3 \lambda \tau$ causes terms of $\cos 3\lambda \tau$ to appear), we assume the stationary solution of the nonlinear system as follows:

$$x(t) = x_0(\mu) \cos \lambda \tau + \mu x_1(\mu) \cos 3\lambda \tau + O(\mu^2), \qquad (18)$$

which means that the higher frequency terms have less and less significance in $x(t)$.

After putting (18) into Eq. (16) and separating the coefficients of $\cos\lambda\tau$, $\cos 3\lambda\tau$, etc. we get:

$$\cos\lambda\tau: \quad (-\lambda^2+1)x_0 + \mu\tfrac{3}{4}x_0^3 = f_0,$$
$$\cos 3\lambda\tau: \quad (-9\lambda^2+1)x_1 + \mu\tfrac{1}{4}x_0^3 = 0,$$
$$\cos 5\lambda\tau: \quad \cdots$$

The equation for the coefficients of $\cos\lambda\tau$ yields the nonlinear amplification diagram in implicit form:

$$(1-\lambda^2)x_0 + \frac{3}{4}\mu x_0^3 - f_0 = 0, \tag{19}$$

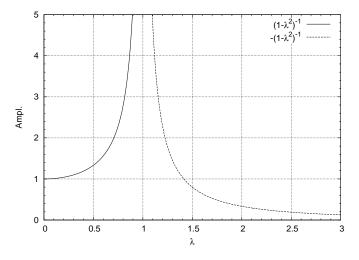from which one can obtain the solution for the linear case ($\mu = 0$) as shown in Eq. (17).

The result of (19) can also be obtained by rewriting Eq. (16) in the following form:

$$x'' + \lambda^2 x = \mu(\Psi x - x^3 + \Phi\cos\lambda\tau), \tag{20}$$

where

$$\Psi = \frac{\lambda^2-1}{\mu}, \quad \Phi = \frac{f_0}{\mu}$$

and applying Poincaré's method ($x(\tau) = x_0(\tau) + \mu x_1(\tau) + \cdots$, etc.).

Fig. 6. Dimensionless amplification diagram for the linear case ($\mu = 0$)
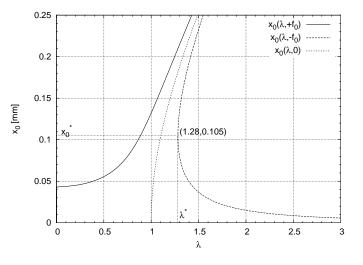
3.3 The nonlinear amplification diagram

The graph of the resonance curve of the linear system is not a continuous function and usually its magnitude is plotted (see Fig. 6):

$$|x_0| = \frac{f_0}{|1-\lambda^2|} \equiv \frac{1}{1-\lambda^2}\begin{cases} +f_0, & \text{if } \lambda < 1 \text{ (left or upper branch)} \\ -f_0, & \text{if } \lambda > 1 \text{ (right or lower branch)} \end{cases}$$

Hence, for nonlinear case ($\mu > 0$) the deformation of these branches is described by the modified forms of Eq. (19), which are also shown in Fig. 7:

$$(1-\lambda^2)x_0 + \frac{3}{4}\mu x_0^3 = +f_0, \text{ (upper branch)} \tag{21}$$
$$(1-\lambda^2)x_0 + \frac{3}{4}\mu x_0^3 = -f_0, \text{ (lower branch)}. \tag{22}$$

Fig. 7. Nonlinear amplification diagram ($f_0 = 0.045$ mm)

In the limit case $f_0 \to 0$ the two branches huddle up against the hyperbola of the so called skeleton curve:

$$\lambda^2 - \frac{x_0^2}{\frac{4}{3\mu}} = 1.$$

One can show that the greater amplitudes ($x_0 > x_0^\star$) of the lower branch belong to unstable solutions and experimentally cannot be detected. It is also interesting to determine the limit frequency $\lambda^\star$ below which only one solution exists, which is stable. This can be achieved by derivating Eq. (22) (lower branch) with respect to x_0 and substituting $\lambda'(x_0^\star) = 0$ into it:

$$1 - (\lambda^\star)^2 + \frac{9}{4}\mu(x_0^\star)^2 = 0. \tag{23}$$

From Eqs. (22) and (23) we obtain:

$$x_0^\star = \sqrt[3]{\frac{2f_0}{3\mu}} \equiv \sqrt[3]{\frac{0.09}{78}} \approx 0.105\,[\text{mm}],$$

$$\lambda^\star = \sqrt{1 + \sqrt[3]{\frac{81}{16}\mu f_0^2}} \approx 1.28.$$

For our physical system this means:

$$\omega^\star = \alpha\sqrt{1 + \sqrt[3]{\frac{81}{16}\mu\left(\frac{Bl n U_0}{sR}\right)^2}} \approx 146\,[\text{Hz}]. \tag{24}$$

4 Experimental results

As the analytical investigations have previously showed, the amplitude of the forced vibration depends on the frequency of the harmonic excitation in the linear and nonlinear case, as well. The perfectness of our mechatronical system model described by Eq. (8) was tested by comparing the vibration curves obtained from numerical simulation and experiments, respectively. It is very important to determine the correct mathematical model (governing equations) and its dynamical parameters in order to design the electronics of the built actuator.

During the experiments, the a displacement amplitude was measured by a transmission opto-gate (TIL 138). Such opto-electronical transducers are typically used in measurements where the displacements are in the submillimeter range. Their main advantage is that they do not influence the object to be measured and they have relatively high cut-off frequency. The results of the experiment and the simulation can be seen in Fig. 8 which shows good agreement. In Fig. 9 the difference from the undamped analytical results can be seen, which is also not too large.
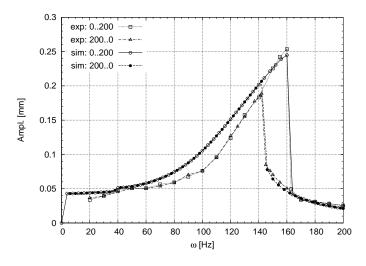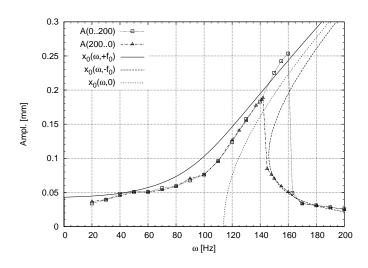
References

1 **Boldea I, Nasar S A**, *Linear Electric Actuator and Generator*, University Press, Cambridge, 1997.

2 **Chung S U, Hwang G Y, Hwang S M**, *Development of brushless and sensorless vibration motor used for mobile phone*, IEEE Transactions on Magnetics **38** (2002), no. 5, 3000–3002.

3 **Farkas M**, *Periodic Motions*, Springer-Verlag, New York, 1994.

4 **Köder T, Schinköthe W**, *Untersuchung zur Zuverlässigkeit von DC Kleinstmotoren*, System-Zuverlässigkeit in frühen Entwicklungsphasen Workshop, September 27, 2004, pp. 1-12.

5 **Linjama J, Kärkkäinen L**, *Modelling and characterization of vibrating alerts*, Nordic Vibration Research, May 11, 2001.

6 **Oesingmann D**, *Entwicklungsrichtungen dauermagneterregter Kommutatormotoren und bürstenlosen Motoren*, 41. Internationales Wissenschaftliches Kolloquium, September 26, 1996, pp. 63-68. Band 2.

7 **Wakiwaka H, Ezawa M, Kato H M, Yoshimura W**, *Development of high-performance millimeter-size vibrator for cellular phones*, Journal of Magnetism and Magnetic Materials (2002), 242-245, 1195-1197. Part 2.

Fig. 8. Amplification diagrams obtained from *exp*eriment and *sim*ulation

5 Conclusions

We have given the mathematical model of an own-developed radial flux linear-motor with air-gap solenoid. We have also proved by numerical simulations that the analytical results based on Poincaré's method of small parameters give us acceptable information on the behaviour of the forced system and the comparison of amplification diagrams showed the correctness of the determined system parameters.

Fig. 9. Comparison of the measured diagram ($A(\omega)$) to the analytical curves ($x_0(\omega, \cdot)$)